Atomistic simulation of dislocation core structure and dynamics in Fe–Ni–Cr–N austenite

M. GRUJICIC
Center for Advanced Manufacturing, Department of Mechanical Engineering, Clemson University, Clemson, SC 29634, USA

Atomistic computer simulations based on the use of the conjugate gradient and molecular dynamics methods were employed to determine the core structure and dynamics of the $a/2\langle 1\,0\,0\rangle$ edge and screw dislocations in Fe–Ni–Cr and Fe–Ni–Cr–N austenites. The embedded-atom method was used to quantify the interactions between iron, nickel, chromium and nitrogen atoms. In Fe–Ni–Cr austenite, both the edge and screw dislocations dissociate along one of the $\{1\,1\,1\}$ planes, forming stacking fault ribbons. The ribbon widths were found to be comparable to their values calculated using the continuum theory. The analysis of dislocation dynamics showed that the phonon drag interferes more with the motion of screw dislocations, reducing their mobility in comparison with the mobility of edge dislocations. In Fe–Ni–Cr–N austenite, the structure of the dislocation core of the $a/2\langle 1\,1\,0\rangle$ edge dislocation does not seem to be significantly affected by the presence of nitrogen. In sharp contrast, the core structure of the dissociated $a/2\langle 1\,1\,0\rangle$ screw dislocation undergoes a major change, resulting in spreading of the core on to two or more non-parallel planes. As a result, mobility of the screw dislocations is substantially lower than that of the edge dislocations. This finding is consistent with the experimental observations that the dislocations are predominantly of the screw character in Fe–Ni–Cr–N austenite.

1. Introduction

The addition of nitrogen into Fe–Ni–Cr austenite is generally found to cause the dislocations to become predominantly screw type [1, 2]. In addition, Fe–Ni–Cr–N alloys show an "unusually" high temperature dependence of flow stress at lower temperatures [3]. These characteristics, the predominance of screw dislocations and the rapid increase in flow stress with decreasing temperature, are typically found in b c c alloys, not in f c c alloys like austenite (e.g. [4]). The behaviour of b c c alloys has been rationalized in terms of lower mobility of the screw dislocations, associated with a non-planar sessile configuration of their core [4–6]. Recently, we reported that the presence of nitrogen can cause similar non-planar dissociation of the $a/2\langle 1\,1\,0\rangle$ screw dislocations in Fe–Ni–Cr austenite [7]. In the present work, the core structure and relative mobility of the $a/2\langle 1\,1\,0\rangle$ edge and screw dislocation in Fe–Ni–Cr and Fe–Ni–Cr–N austenites were analysed using atomistic simulations. The simulations of the dislocation core structure were done at 0 K using the conjugate gradient method [8] to minimize the potential energy of the crystal with respect to the atoms positions. Dislocation dynamics was studied using molecular dynamics simulations.

2. Embedded-atom method

The embedded-atom method (EAM) was originally developed by Daw and Baskes [9, 10], and its theory and application have recently been reviewed [11]. In the EAM the potential energy, E_{pot}, of a system containing nitrogen atoms is defined as

$$E_{\text{pot}} = \sum_{i=1}^{N} F_i(\rho_i) + \sum_{\substack{i<j \\ i,j=1}}^{N} \phi_{ij}(r_{ij}) \tag{1}$$

where $F_i(\rho_i)$ is the energy to embed an atom in the electron density, ρ_i, at the location of atom i, and $\phi_{ij}(r_{ij})$ is the two-body Coulombic interaction potential between atoms i and j separated by a distance r_{ij}. The electron density, ρ_i, at the location of atom i is given by a linear superposition of spherically averaged atomic densities of all other atoms in the system, ρ_j^{a}, as follows

$$\rho_i = \sum_{j \neq 1} \rho_j^{\text{a}}(r_{ij}) \tag{2}$$

The atomic densities are generally determined using the Hartree–Fock theory and double-zeta electron density functions as tabulated by Clementi and Roetti [12].

The $\phi_{ij}(r_{ij})$ potential is typically represented as

$$\phi_{ij}(r_{ij}) = Z_i(r_{ij})\, Z_j(r_{ij})/r_{ij} \tag{3}$$

where Z_i and Z_j are, respectively, the effective charge functions for atoms i and j which are positive quantities and which decrease monotonically with the interatomic distance r_{ij}.

0022–2461

Using experimental data for the cubic elastic constants, the cohesion energies, the equilibrium lattice parameters, and the heats of mixing in the limit of infinite dilution, Grujicic and Zhou [11] recently determined the $F_i(\rho_i)$, $\rho(r_{ij})$ and $\phi_{ij}(r_{ij})$ functions for iron, nickel, chromium and nitrogen in the Fe–Ni–Cr–N austenitic steels. These functions have been utilized in the present paper to quantify the atomic interactions within the computational crystal used in the atomistic simulations.

Our preliminary results showed that the structure of the dislocation core in the Fe–Ni–Cr austenite is somewhat affected by the local chemical composition and the atomic order. In order to separate this effect from the effect of nitrogen on the dislocation core structure, we applied the effective atom method in which the metallic sublattice in the austenite is regarded as if it contains identical (effective) metallic atoms [11, 13]. The embedding energy and the electron density functions for the effective (metallic) atoms are defined as a weighted average of the corresponding functions for iron, nickel and chromium

$$F_{\text{eff}}(\rho) = \sum_{i=\text{Fe, Ni, Cr}} y_i F_i(\rho) \tag{4}$$

$$\rho_{\text{eff}}(r) = \sum_{i=\text{Fe, Ni, Cr}} y_i \rho_i(r) \tag{5}$$

The effective pair potential function is defined as a weighted average of the pair potentials between iron, nickel and chromium and their "average" neighbours. That is

$$\phi_{\text{eff}}(r) = \sum_{i=\text{Fe, Ni, Cr}} y_i \phi_{i\alpha}(r) \tag{6}$$

where

$$\phi_{i\alpha}(r) = \sum_{j=\text{Fe, Ni, Cr}} y_j \phi_{ij}(r) \quad \text{for } i = \text{Fe, Ni, Cr} \tag{7}$$

Substitution of Equation 7 into Equation 6 yields

$$\phi_{\text{eff}}(r) = \sum_{i=\text{Fe, Ni, Cr}} \sum_{j=\text{Fe, Ni, Cr}} y_i y_j \phi_{ij}(r) \tag{8}$$

where y is the site fraction of iron, nickel or chromium on the metallic sublattice.

Based on Equations 3 and 8, the effective charge function for the effective atoms is

$$Z_{\text{eff}}(r) = \left[\sum_{i=\text{Fe, Ni, Cr}} \sum_{j=\text{Fe, Ni, Cr}} y_i y_j Z_i(r) Z_j(r) \right]^{1/2} \tag{9}$$

Using Equations 4, 5, 8 and 9 and the $F_i(\rho_i)$, $\rho_i(r)$, $\phi_{ij}(r)$ and $Z_{ij}(r)$ functions for iron, nickel and chromium from our previous work [11], the effective functions $F_{\text{eff}}(\rho)$, $\rho_{\text{eff}}(r)$, $\phi_{\text{eff}}(r)$ and $Z_{\text{eff}}(r)$ were determined.

To avoid surface effects and simulate the behaviour of an infinite dislocation, periodic boundary conditions were applied in the direction parallel to the dislocation line. When nitrogen is introduced into the computational crystal to study its effect on the dislocation structure, due to periodic boundary conditions, nitrogen atoms form an infinite row of atoms parallel to the dislocation line. Under such circumstances, in order to obtain a realistic line concentration of nitrogen, the periodic length of the computational crystal in the dislocation line direction would have to be increased significantly making the size of the computational crystal prohibitively large and the computation impractical. The maximum size of the computational crystal studied in the present work allowed us to place nitrogen into every other interstitial site along the direction of the dislocation line. It must be noted that because this resulted in an unphysically large concentration of nitrogen atoms, the results to be obtained could be used only for a qualitative analysis of the effect of nitrogen.

3. Computational procedure

3.1. Computational crystal and dislocation generation

3.1.1. Edge dislocation

A rectangular computational crystal containing initially 5148 atomic sites arranged on two interpenetrating fcc lattices was used to study the core structure and mobility of the edge $a/2\langle 1\,1\,0\rangle$ dislocation. The orientation and the size of the crystal are given in Fig. 1. The edge sizes are expressed in terms of the number of non-equivalent $(\bar{2}\,2\,0)$, $(1\,1\,1)$ and $(2\,2\,\bar{4})$ planes in either of the two sublattices. Initially, equivalent (metallic) atoms were placed onto one of the fcc lattices and the potential energy of the crystal minimized subject to flexible periodic boundary conditions along all three principal directions. This procedure yielded the equilibrium lattice parameter 0.353 41 nm at 0 K. All the subsequent calculations were done under the condition that the lattice parameter remains fixed.

To generate an $a/2[\bar{1}\,1\,0]$ edge dislocation, two neighbouring $[\bar{2}\,2\,0]$ halfplanes were removed from the bottom half of the crystal. This procedure reduced the total number of atoms to 5172. To help the resulting edge dislocation dissociate into two Shockley partial dislocations, one of the adjacent $(\bar{2}\,2\,0)$ halfplanes was shifted into the position of one of the "missing" halfplanes, Fig. 1. This resulted in a one-plane separation of the two missing (or extra) $(2\,2\,0)$ planes. Minimization of the potential energy of this configuration, causes further separation of the two extra halfplanes, i.e. further separation of the two Shockley partial

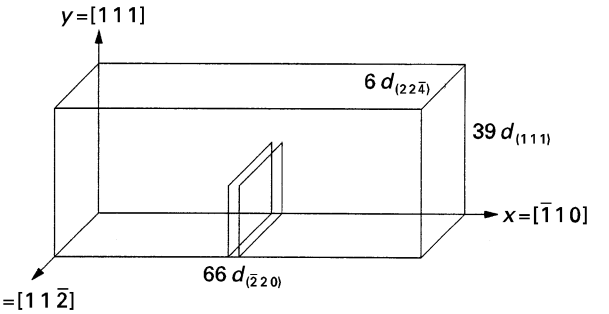

Figure 1 Geometry and size of the computational crystal used in the analysis of the $a/2[\bar{1}\,1\,0]$ edge dislocation. Two $(\bar{2}\,2\,0)$ halfplanes indicated in the figure were removed in order to generate the edge dislocation.

dislocations. All the calculations of the core structure and dynamics were done under the periodic boundary condition in the [1 1 $\bar{2}$] and [$\bar{1}$ 1 0] directions, and the free-surface boundary condition in the [1 1 1] directions and hence pertain to the case of a single infinitely long edge dislocation.

3.1.2. Screw dislocation

The geometry and the size of the computational crystal used in the analysis of the $a/2\langle 1\,1\,0\rangle$ screw dislocation is shown in Fig. 2. The block contained 5320 atomic sites arranged on two interpenetrating f c c lattices. The size of the computational crystal is again given in terms of the number of non-equivalent ($\bar{2}$ 2 4), (1 $\bar{1}$ 1) and (2 2 0) planes. Using the aforementioned procedure, the equilibrium lattice parameter at 0 K was obtained again. As expected, the same value for the lattice parameter ($a = 0.354$ nm) was obtained for both computational crystals. The lattice parameter was fixed at this value in all the subsequent calculations.

To generate a screw dislocation along the [1 1 0] direction, atoms were displaced from their perfect positions (x, y) in the [1 1 0] direction by a distance w, according to the formula

$$w = \frac{\boldsymbol{b}}{2\pi} \arctan \frac{y - y_0}{x - x_0} \tag{10}$$

where $\boldsymbol{b}$ is the magnitude of the Burgers vector, (x_0, y_0) the coordinates of the dislocation centre. In our previous work [7] we explored the effect of various elastic centres of the dislocation on its energy and found that the dislocation centre marked Δ in Fig. 6a (see later) is associated with the lowest energy. Hence only this screw dislocation configuration was analysed in the present paper. As discussed elsewhere [7], to initiate dissociation of the unit $a/2$[1 1 0] screw dislocation, the flexible, periodic boundary conditions were initially applied along all three principal directions in Fig. 2, and the potential energy of the crystal minimized. After the dislocation has dissociated, the free surface boundary conditions were next applied along the two directions ([$\bar{1}$ 1 2] and [1 $\bar{1}$ 1]) normal to the dislocation line and the energy minimization procedure repeated. This yielded a minor change in the energy and no apparent change in the stacking fault ribbon width. All the subsequent calculations were carried out under the periodic boundary condition in the [1 1 0] and [$\bar{1}$ 1 2] directions and the free surface conditions in the [1 $\bar{1}$ 1] direction and thus pertain to the case of a single, infinitely long screw dislocation.

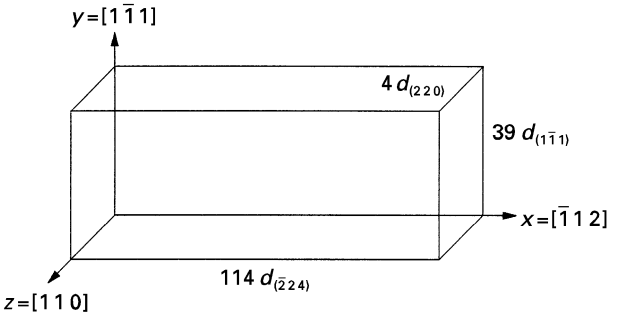

Figure 2 Geometry and size of the computational crystal used in the analysis of the $a/2$[1 1 0] screw dislocation.

3.2. Analysis of the dislocation core

3.2.1. Edge dislocation

According to Fig. 1, the line direction of the $a/2$[$\bar{1}$ 1 0] edge dislocation is [1 1 $\bar{2}$]. To analyse the dislocation core it is convenient to use a projection of the atoms on the plane normal to the dislocation line, the (1 1 $\bar{2}$) plane in this case. A (1 1 2) projection of the atoms in the f c c structure is given in Fig. 3a. It should be noted that there are six non-equivalent (2 2 $\bar{4}$) planes projected in Fig. 3a. However, the analysis carried out here did not entail the use of separate symbols to discriminate between the atoms belonging to different non-equivalent (2 2 $\bar{4}$) planes.

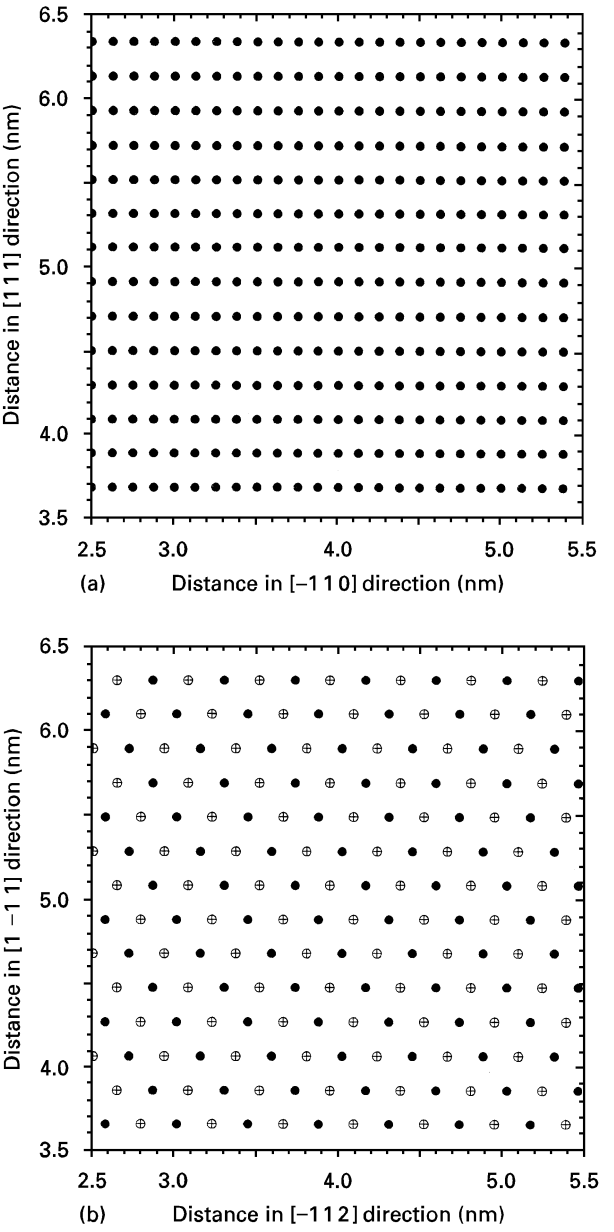

Figure 3 (a) (1 1 $\bar{2}$) projection, and (b) (1 1 0) projection, of atoms in the f c c crystal.

To display the structure of the dissociated edge dislocation core, edge-type and screw-type relative atomic displacements were determined and shown separately. The edge-type relative displacement of the two atoms is represented by a vector centred at the midpoint of the two atoms, and having the length proportional to the magnitude of the $(1\,1\,\bar{2})$ projection of the relative displacement vector of the two atoms. The arrow on the edge-type relative displacement vector refers to the direction of the edge-type relative displacement of the atom with a larger value of its y coordinate. If the y coordinates of the two atoms are the same, then the arrow refers to the displacement of the atom with a larger x coordinate.

The screw-type relative displacement is represented by a vector centred at the midpoint and lying along the line connecting the two atoms. Its magnitude is proportional to the relative $[1\,1\,\bar{2}]$ displacement of the two atoms and the arrow points to the atoms whose relative displacement is in the positive $[1\,1\,\bar{2}]$ direction.

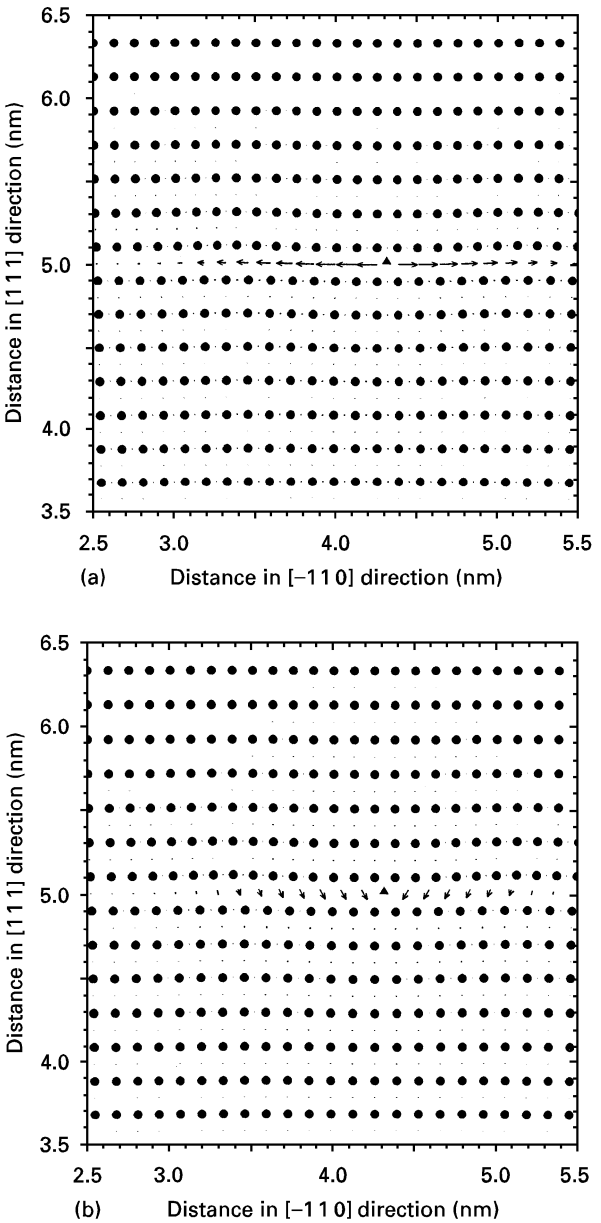

Figure 4 (a) Edge-type, and (b) screw-type, relative atomic displacements associated with a dissociated $a/2[1\,1\,0]$ edge dislocation. Fe–Ni–Cr alloy.

Determination of the relative displacements associated with an edge dislocation must be done very carefully because the number of atoms above and below the slip plane is not the same. In the present work, the following procedure was used. The relative differential displacements are determined starting in the region far away from the dislocation (say, at the left side of the computational crystal), where the crystal is nearly perfect and hence the relative displacement is negligible, Fig. 4a and b. On moving towards the dislocation, the magnitude of the relative displacements increases. When the magnitude of the edge-type relative displacement becomes larger or equal to $\boldsymbol{b}/2 = |a/4[\bar{1}\,1\,0]|$, two $[\bar{2}\,2\,0]$ extra halfplanes are skipped while calculating the displacements of the atoms above the slip plane relative to the atoms below the slip plane. Because the screw-type relative displacement vectors lie along the line connecting the two atoms in question, the procedure described above can be easily understood with the help of Fig. 4b.

3.2.2. Screw dislocations

To analyse the structure of the dissociated screw dislocation core, it is again convenient to use an atomic projection on the plane normal to the dislocation line, the $(1\,1\,0)$ plane in this case. A $(1\,1\,0)$ projection of the atoms is given in Fig. 3b, where two different circles are used to distinguish the atoms belonging to two non-equivalent $(2\,2\,0)$ planes.

The edge-type relative displacements were defined in the same way as in the case of a dissociated edge dislocation. However, the procedure was somewhat simpler to implement in this case because the number of atoms below and above the slip plane were the same. For convenience, the edge-type relative displacements were scaled relative to the magnitude of the edge component of the Burgers vector of a Shockley partial, $|a/4[\bar{1}\,1\,2]|$ in this case.

The screw-type relative displacements were defined in the same fashion as in the case of a dissociated edge dislocation. However, they are scaled in this case so that when their magnitude is $\boldsymbol{b}/2 = |a/4[1\,1\,0]|$, the screw-type relative displacement vector just touches the two atoms. When the relative displacement exceeds $\boldsymbol{b}/2$, due to the crystal periodicity, it is convenient to have the arrow point towards the other atom.

3.3. Dislocation dynamics

The glide of a single, dissociated (edge or screw) $a/2\langle 1\,1\,0\rangle$ dislocation due to application of the shear stress (parallel to the slip plane and in the direction of the Burgers vector) at different temperatures has been studied by performing standard molecular dynamics calculations. The temperature was attained by giving each atom an initial random velocity chosen from a Boltzmann distribution. Equipartition of kinetic and potential energy occurred in ~ 0.1 ps. The temperature was maintained by exponential relaxation at each time step (2×10^{-15} s or 2 fs) of the average

squared velocity i.e. temperature to the desired temperature using a time constant of 0.1 ps. This procedure allowed the temperature to be kept within a range of 3% of the target temperature. The shear stresses, τ_{xy} for the edge and τ_{zy} for the screw dislocation, were introduced by applying the external forces to the boundary atoms on the free surfaces. The location of the moving dislocation was monitored using the relative atomic displacement discussed in Section 3.2. The calculations were carried out to three stress levels (10, 30 and 60 MPa) and at three temperatures (10, 50 and 100 K).

4. Results and discussion

While the procedure developed here is quite general and can be applied to any Fe–Ni–Cr–N f c c alloy, our calculations were confined to Fe–40 Ni–15 Cr wt % without and with nitrogen. The metal atom site fractions ($y_{Fe} = 0.4538$, $y_{Ni} = 0.3838$ and $y_{Cr} = 0.1625$) are the same in the alloys without and with nitrogen. The reason for choosing these alloys was two-fold: (a) we are currently conducting the tensile tests on single crystals of these alloys at low temperatures and plan ultimately to correlate the experimental data with our atomistic simulation results, and (b) in our previous work [14] we carried out a detailed analysis of the short-range order in the two alloys using Monte-Carlo simulations, and hope by gathering various information for the same alloy systems to be able better to elucidate the role of nitrogen in Fe–Ni–Cr austenite.

4.1. Fe–40Ni–15Cr alloy without nitrogen

4.1.1. Dislocation core structure

Fig. 4a and b show the equilibrium configuration of the core of an $a/2\,[\bar{1}\,1\,0]$ edge dislocation in the Fe–40 Ni–15 Cr alloy at 0 K. The dislocation core spreads along the (1 1 1) plane creating a stacking fault ribbon which is bound by two Shockley partial dislocations. This dislocation dissociation can be represented as follows

$$a/2[\bar{1}\,1\,0] = a/6[\bar{1}\,2\,\bar{1}] + a/6[\bar{2}\,1\,1] \qquad (11)$$

The Burgers vector of each of the two Shockley partials, can be represented as a sum of its edge and screw components as follows

$$a/6[\bar{1}\,2\,\bar{1}] = a/4[\bar{1}\,1\,0]_e + 1/12\,[1\,1\,\bar{2}]_s \qquad (12)$$

$$a/6[\bar{2}\,1\,1] = a/4[\bar{1}\,1\,0]_e + 1/12\,[\bar{1}\,\bar{1}\,2]_s \qquad (13)$$

The two partials thus differ in the character of the screw component of their Burgers vector. A careful examination of the screw-type relative displacement map, Fig. 4b, shows that the Shockley partial on the left is of the $a/6[\bar{1}\,2\,\bar{1}]$ type, while the Shockley partial on the right is of the $a/6[\bar{2}\,1\,1]$ type.

According to the (isotropic) continuum theory, the width of a stacking fault ribbon, d_{SF}, is given as [15]

$$d_{SF} = \frac{\mu \boldsymbol{b}^2}{8\pi E_f} \frac{2-\nu}{1-\nu}\left(1 - \frac{2\nu}{2-\nu}\cos 2\beta\right) \qquad (14)$$

where μ is the shear modulus, $\boldsymbol{b}$ the magnitude of the Burgers vector of either of the two partials, E_f the stacking fault energy, ν Poisson's ratio and β the angle between the line direction of the undissociated dislocation and its Burgers vector. Using the following data: $\mu = 65$ GPa [11], $E_f = 80\,\mathrm{mJ\,m^{-2}}$ (present work), $6 = \sqrt{6}/6a$, $a = 0.3574$ nm (present work), $\nu = 0.3$ and $\beta = 90^\circ$, we obtained $d_{SF} = 2.26$ nm. This is in excellent agreement with the $d_{SF} \approx 2.3$ nm as seen in Fig. 4a and b. The value $\mu = 0.65$ GPa is obtained as a Voigt average of the shear modulus based on the single-crystal elastic constants C_{11}, C_{12} and C_{44} computed using the EAM functions presented in Section 2.

The stacking fault energy was computed using the following procedure. The upper half of the (perfect) crystal shown in Fig. 2, was shifted (rigidly) by one Burgers vector of the Shockley partial dislocation, $a/6$ [1 2 1] and the resulting configuration relaxed by minimizing the potential energy of the crystal subject to the periodic boundary conditions. The magnitude of the stacking fault energy was then computed by dividing the difference in the energies of the faulted and the perfect crystal by the area of the stacking fault (twice the area of the x–z face). The computed value of the stacking fault energy, $80\,\mathrm{mJ\,m^{-2}}$ is in excellent agreement with its experimental counterpart, $75\,\mathrm{mJ\,m^{-2}}$ [16].

Fig. 5a and b show the equilibrium configuration of the core of the $a/2[1\,1\,0]$ screw dislocation in the Fe–40 Ni–15 Cr alloy at 0 K. The dislocation dissociates along the $(1\,\bar{1}\,1)$ plane creating a stacking fault ribbon which is bound by two Shockley partial dislocations. This process can be represented as

$$a/2[1\,1\,0] = a/6[1\,2\,1] + a/6[2\,1\,\bar{1}] \qquad (15)$$

The Burgers vector of each of the two partials can be represented by a sum of its edge and screw components as follows

$$a/6[2\,1\,\bar{1}] = a/4[1\,1\,0]_s + a/12[1\,\bar{1}\,\bar{2}]_e \qquad (16)$$

$$a/6[1\,2\,1] = a/4[1\,1\,0]_s + a/12[\bar{1}\,1\,2]_e \qquad (17)$$

The two partials thus differ in the character of the edge component of their Burgers vector. A careful examination of the edge-type relative displacement map, Fig. 5(b), shows that the Shockley partial on the left is of the $a/6[1\,2\,1]$ type and that on the right is of the $a/6[2\,1\,\bar{1}]$ type.

Setting $\beta = 0$ and holding the remaining parameters on the right-hand side of Equation 14 at their previous values, the width of the stacking fault ribbon in the case of a dissociated screw dislocation was found to be ~ 1.08 nm. Again, this is in excellent agreement with the observed width of the stacking fault ribbon ~ 1.3 nm, in Fig. 5a and b.

The dislocations core structures in Fe–40Ni–15Cr shown in Figs 4a, b and 5a, b are quite common to non-ordered f c c metals as observed in a number of previous studies (e.g. [17]). The core structure is principally governed by crystallography (the slip plane and the slip direction) and by the magnitude of the stacking fault energy, with the latter being the only (interatomic) potential controlled parameter. While

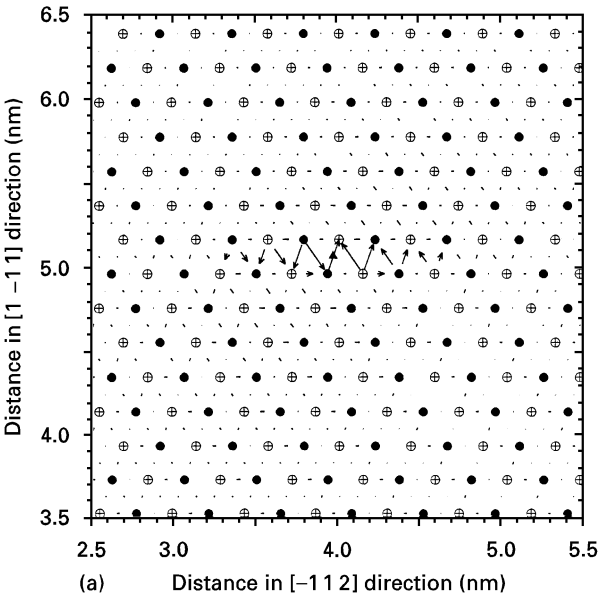

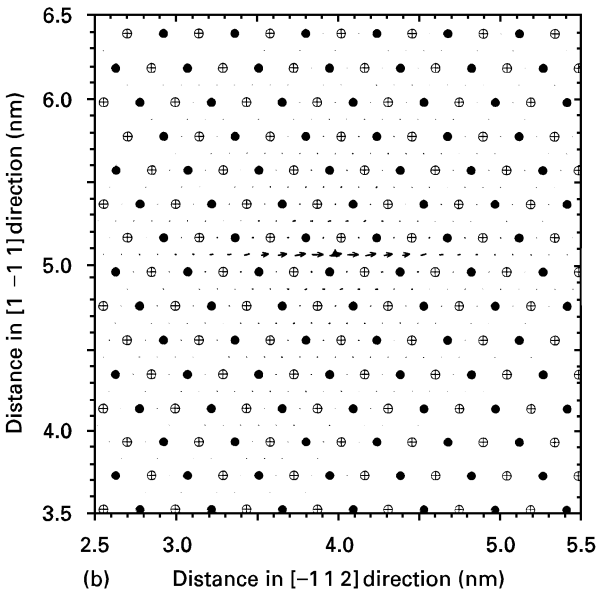

Figure 5 (a) Screw-type, and (b) edge-type, relative atomic displacements associated with a dissociated $a/2[1\,1\,0]$ screw dislocation. Fe–Ni–Cr alloy.

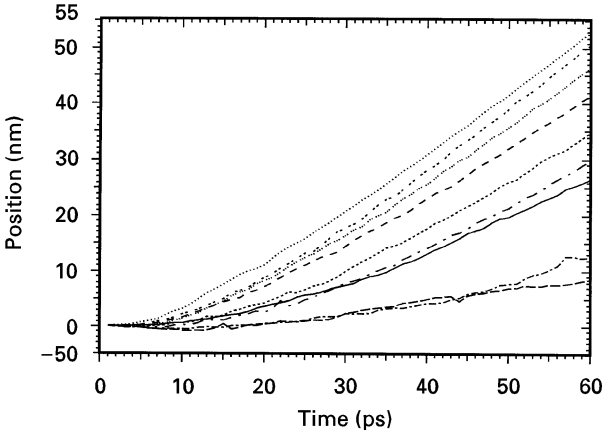

Figure 6 Position of the dissociated $a/2[1\,1\,0]$ edge dislocation as a function of time. Fe–Ni–Cr alloy. 10 K: (——) 15 MPa, (– – –) 30 MPa, (···) 60 MPa. 50 K: (–·–) 15 MPa, (- - -) 30 MPa, (- - - - -) 60 MPa. 100 K: (– – –) 15 MPa, (—·—) 30 MPa, (··· ··· ···) 60 MPa.

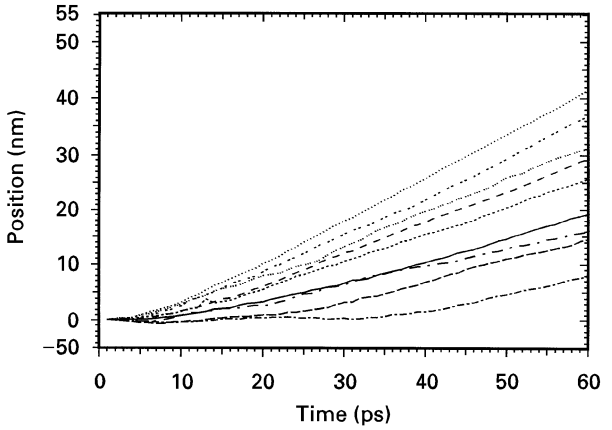

Figure 7 Position of the dissociated $a/2\,[1\,1\,0]$ screw dislocation as a function of time. Fe–Ni–Cr alloy. For key, see Fig. 6.

the results shown in Figs 4a, b and 5a, b could have been obtained within the framework of continuum theory of dislocations, it was critical to reproduce them using the atomistic computer simulations in order to verify the validity of the interatomic potential functions used in the present simulations.

4.1.2. Dislocation dynamics

Figs 6 and 7 show, respectively, the position of an edge and a screw $a/2\langle 1\,1\,0\rangle$ dislocation as a function of time in the molecular dynamics run at the shear stress levels of 10, 30 and 60 MPa and at three temperatures: 10, 50, and 100 K. The results indicate that from the start, the dislocation begins to accelerate and ultimately attains a constant velocity whose magnitude depends on stress and temperature.

According to continuum theory, the dislocation dynamics can be described by the following differential equation [18]

$$\frac{\mathrm{d}}{\mathrm{d}t}\frac{m\nu}{[1-(\nu/c)^2]^{1/2}} = (\tau-\tau_0)\boldsymbol{b} - \alpha\frac{3kT}{10\boldsymbol{b}^2}\frac{\nu/c}{[1-(\nu/c)^2]^{1/2}} \tag{18}$$

where ν and m are, respectively, the dislocation velocity and the dislocation mass per unit length, c is a limiting velocity, τ is the applied shear stress, τ_0 the lattice frictional stress, $\boldsymbol{b}$ the Burgers vector, α a dimensionless constant, and k and T have their usual meanings. The right-hand side in the above equation represents the net driving force, i.e. the difference between the applied driving force and the resisting (lattice friction and phonon drag) forces to the dislocation motion. To determine four parameters (c, m, a and τ_0) in the above equation, Equation 18 was first solved analytically for the dislocation velocity and then numerically for the dislocation position as a function of time. The least-squares fitting was next applied to the data shown in Figs 6 and 7 to determine the four parameters. The results of this fitting procedure are given in Table I.

The dislocation mass and frictional stress shown in Table I have apparently the same values for the edge and screw dislocations. In addition, their magnitudes

TABLE I Dislocation dynamics parameters in Fe–Ni–Cr

Parameter	Edge dislocations	Screw dislocations
c (nm ps^{-1})	1.4	0.9
m (atoms/Burgers' distance)	0.21	0.22
α	1.2	1.8
τ_0 (MPa)	3.1	3.1

appear quite reasonable. For instance, in f c c metallic materials, the critical shear stress associated with the onset of plastic deformation, τ_c, is of the order of 10^{-5} to 10^{-4} μ. Thus, for $\mu = 65$ GPa, $\tau_c = 0.65$–6.5 MPa. The magnitude of the frictional stress, $\tau_0 = 3.1$ MPa, obtained in the present work falls within this range. The scaling factor for the drag term, α, on the other hand, is significantly larger for the screw than for the edge dislocations. As a consequence, the limiting velocity, c, i.e. the terminal dislocation velocity at very high stress levels, $\tau \gg \tau_0$, is lower for the screw than for the edge dislocations. In fact, our results show that at any level of applied stress $\tau > \tau_0$, the terminal dislocation velocity for the screw dislocations is lower than that for the edge dislocations. This suggests that the dissociated $a/2\langle 1\,1\,0\rangle$ edge dislocations are more mobile than their dissociated screw counterparts. This finding is consistent with the results shown in Figs 4 and 5, which indicate that the core of the edge dislocations is spread to a greater extent along the slip plane when compared to that of the screw dislocations. As a result, the motion of the edge dislocations is associated with smaller displacements of the atoms in their core and, hence, encounters less resistance from the lattice.

The results shown in Figs 6 and 7 indicates that the mobility of dislocations decreases as temperature is increased. In fact, we observed that at temperatures in excess of 400 K and at stress levels up to 60 MPa (results not shown for brevity), no large-scale motion of the dislocation takes place during several simulation runs of 200 ps. This finding confirms what is already implied by Equation (14), that the motion of dislocations is controlled by their interaction with (thermally excited) phonons. That is, at lower temperatures (up to 100 K), the net driving force (the difference between the applied and the resisting forces) on the dislocation is positive and the dislocation dynamics is described by Equation (14). At higher temperatures, on the other hand, thermally excited phonons appear to give rise to an additional "friction-like" term. As a result, the net driving force on the dislocation becomes negative and the forward motion of the dislocation requires thermal activation. Under such circumstances, dislocation motion is expected to be controlled by kink formation over the primary Peierls barrier and (lateral) kink propagation across the secondary Peierls barrier. There are two reasons why such dislocation motion was not observed in our simulations at 400 K: (a) the average dislocation velocity in the thermally activated regime is too small for a dislocation to advance one periodic distance during the time of 200 ps, and (b) the periodic boundary conditions used in our simulations enhance the barrier to the process of kink formation by limiting the maximum length (hence increasing the curvature) of the kink.

4.2. Fe–40 Ni–15 Cr alloy with nitrogen

As demonstrated in our previous work [7], the details of the way nitrogen affects the core structure of an $a/2\langle 1\,1\,0\rangle$ screw dislocation vary with the relative position of the nitrogen atom and the dislocation. However, a particular feature, that is spreading of the dislocation core on to two non-parallel $\{1\,1\,1\}$ planes containing the dislocation line, was found to be common to all the configurations. For an $a/2\langle 1\,1\,2\rangle$ edge dislocation, we found that the effect of nitrogen on the structure of the dislocation core is much less sensitive to the relative position of the nitrogen atoms and the dislocation. Therefore, in the present paper we compare the effect of nitrogen on the core structure and mobility of $a/2\langle 1\,1\,0\rangle$ edge and screw dislocations for a fixed relative position of the nitrogen atoms and the dislocation. Specifically, a row of nitrogen atoms was placed on the slip plane just ahead of the leading Shockley partial dislocation both for the case of a dissociated $a/2[\bar{1}\,1\,0]$ edge dislocation and a dissociated $a/2[1\,1\,0]$ screw dislocation.

4.2.1. Dislocation core structure

The effect of nitrogen atoms, placed on the slip plane just ahead of the leading Shockley partial dislocation, on the core structure of the dissociated $a/2[\bar{1}\,1\,0]$ edge dislocation is shown in Fig. 8a and b. Nitrogen causes minor lattice distortions, but does not change the structure of the dislocation core significantly. In particular, the dislocation remains spread on the slip plane. Similar results were obtained when a row of nitrogen atoms was placed above or below the slip plane, and hence will not be shown here.

The effect of nitrogen atoms, placed on the slip plane just ahead of the leading Shockley partial dislocation, on the core structure of the dissociated $a/2[1\,1\,0]$ screw dislocation is shown in Fig. 9a and b. Nitrogen causes spreading of the dislocation core on to two close packed planes, $(1\,\bar{1}\,1)$ and $(\bar{1}\,1\,1)$. As discussed in our previous work [7], this dislocation process can be described as

$$a/2[1\,1\,0] = a/6[1\,2\,1] + a/6[1\,2\,\bar{1}] + a/6[1\,\bar{1}\,0] \quad (19)$$

The dislocation with the Burgers vector $a/6[1\,\bar{1}\,0]$ is of the edge type and its slip plane is $(0\,0\,1)$. Because $(0\,0\,1)$ is not a close-packed plane, glide of the $a/6[1\,\bar{1}\,0]$ dislocation requires a higher stress, and hence the entire dissociated $a/2[1\,1\,0]$ screw dislocation is less mobile.

One might argue that modelling the interaction of one infinite row of nitrogen atoms with a parallel dislocation (a fairly improbable configuration in the real material) may furnish little useful information about the phenomenon of nitrogen strengthening. Owing to a low solubility of nitrogen in austenite, it

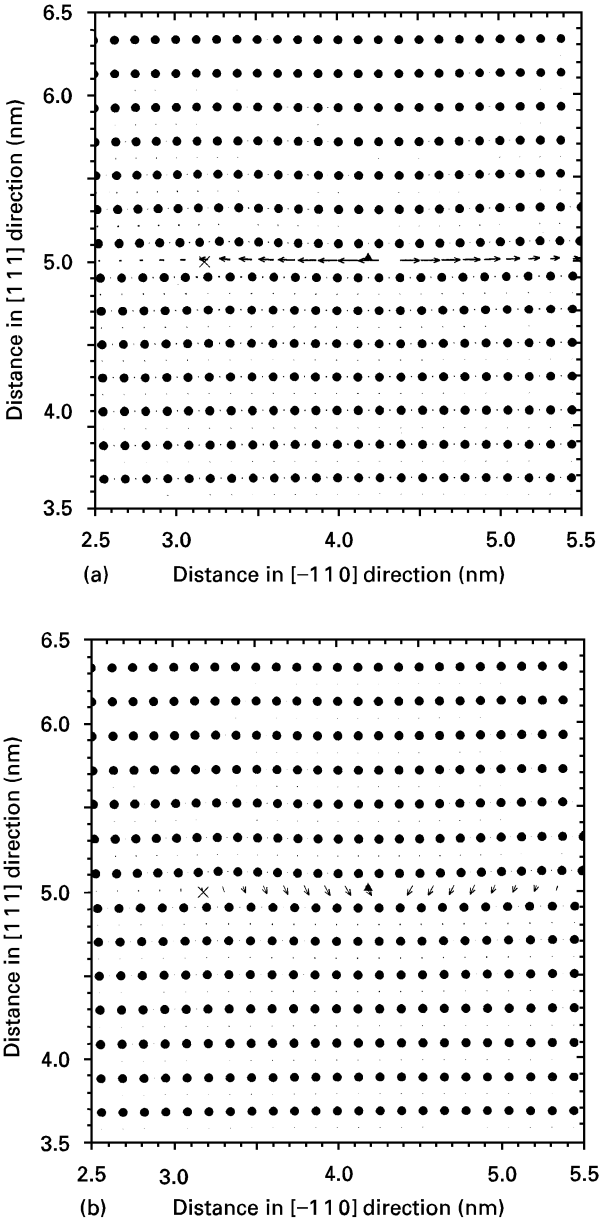

Figure 8 (a) Edge-type, and (b) screw-type, relative atomic displacements associated with a dissociated $a/2[\bar{1}\,1\,0]$ edge dislocation. Fe–Ni–Cr–N alloy.

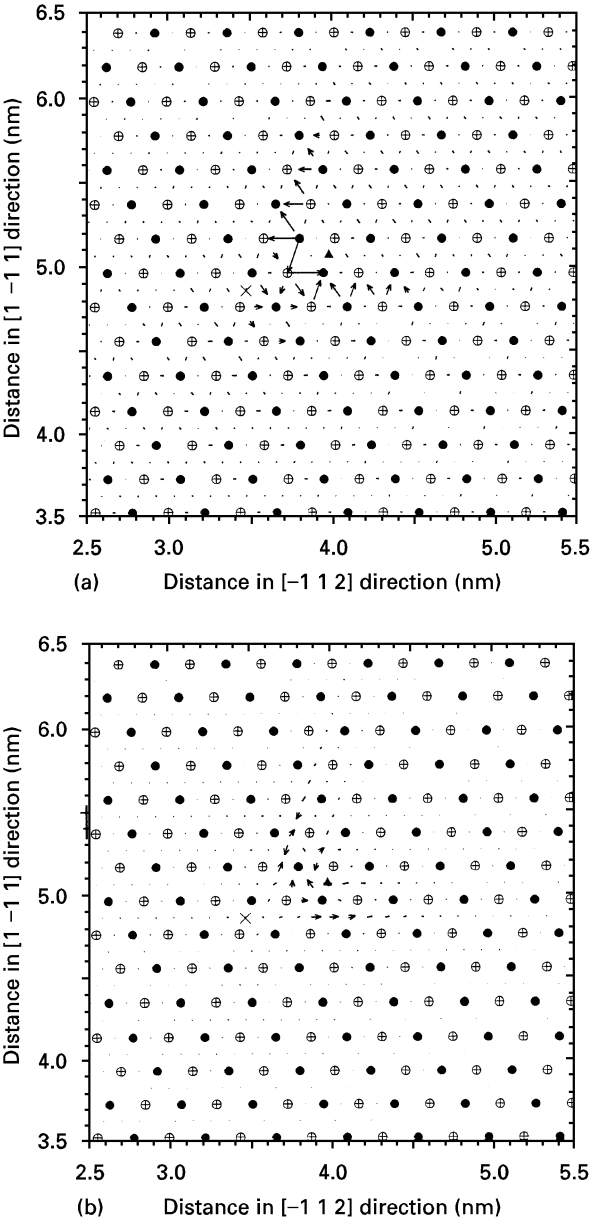

Figure 9 (a) Screw-type, and (b) edge-type, relative atomic displacements associated with a dissociated $a/2[1\,1\,0]$ screw dislocation. Fe–Ni–Cr–N alloy.

appears that modelling the interaction of a single nitrogen atom with the dislocation may provide more insight into the problem. However, such three-dimensional modelling would require the use of a prohibitively large computational crystal and could not be carried out. We found that spreading of the screw dislocation core on to two non-parallel close packed planes takes place (although the extent is somewhat lower) not only when the nitrogen atoms are placed into every interstitial site but also when the nitrogen is put into every other interstitial site along the infinite row. This finding suggests that the interaction of the dislocation with isolated nitrogen atoms can locally change the dislocation core structure. The segments of the screw dislocation with the non-planar core structure are expected to have lower mobility than the rest of the dislocation line and are expected to act as "pinned" segments. As a consequence, the mobility of the screw dislocations is expected to be lower than that of the edge dislocations. This, in turn, can be used to explain why there are screw dislocations predominantly found in the Fe–Ni–Cr austenite containing nitrogen [19].

The effect of nitrogen on the dynamics of the edge dislocations (results not shown for brevity) was found to be very sensitive to the relative position of nitrogen atoms and the dislocation. By applying the fitting procedure described in the previous section, however, it was found that only the frictional stress, τ_0, was increased from 3.1 to $\sim$4.0 MPa while the other dynamics parameters, c, m and α remained closed to their respective counterparts in Fe–Ni–Cr austenite, Table I.

Owing to the complex core structure which undergoes large changes during dislocation motion, it was very difficult to monitor the progress of the screw

dislocation motion. However, the velocity of the screw dislocations at a given stress and temperature was estimated to be typically lower by about one order of magnitude when compared to that for the edge dislocations in Fe–Ni–Cr–N austenite. Again, it should be noted that due to the use of periodic boundary conditions, the results obtained in the present work pertain to relative mobility of the straight, edge and screw, dislocations. The results suggest that in the high-velocity drag-controlled regime, because of the non-planar character of their core structure, the straight screw dislocations are less mobile than their edge counterparts. On the other hand, under more common plastic deformation conditions, the average dislocation velocity is several orders of magnitude lower and controlled by thermal activation of the kink formation and the kink propagation processes. As discussed earlier, atomistic simulation of the latter processes is not feasible at the present time. Then, one must ask whether our results pertaining to the core structure and the hopping motion of straight dislocations, can tell us anything about the mobility of dislocations via the kink mechanism. We believe that the answer is positive and that the "pinned" segments formed along the screw dislocations interfere with both the formation and the propagation of the kinks, making these dislocations less mobile. This can be explained by the following: because of the formation of the pinned segments, the length of the free dislocation segments, the segments which bow out under applied stress and participate in the kink formation process, is reduced in the case of the screw dislocations. Because, at a constant stress, the maximum forward excursion of the bowed out segment scales roughly with the segment length, such excursion is smaller and consequently the probability for kink formation is lower for the screw dislocations. Furthermore, once the kinks are nucleated, their lateral motion along the dislocation line is hampered by the presence of pinned segments, giving rise to their lower velocity. Because the velocity of the dislocations in the thermally activated regime scales with the product of the probability for kink formation and the kink velocity and the latter two are expected to be smaller in the case of the screw dislocations, one should expect lower mobility of the screw dislocations in Fe–Ni–Cr–N. This conclusion is consistent with the experimental findings (e.g. [19]) that the dislocations are predominantly of the screw character in these alloys.

It should be noted that the interstitial strengthening of f c c alloys is often attributed to the (dilational) strain interaction between the dislocations and the interstitials (e.g. [20]). Accordingly, the first-order strain interaction between an interstitial and the screw dislocation is zero and only the edge dislocations contribute to interstitial strengthening. Our findings reported here, however, suggest that the strain interaction of nitrogen atoms with the edge dislocation may not represent the dominant part of interstitial strengthening. This is supported by X-ray diffraction measurements [1] which show that nitrogen-induced dilational strains in Fe–Ni–Cr austenite are relatively small and symmetric.

5. Conclusion

EAM-based atomic simulations show that both the edge and the screw $a/2\langle 1\,1\,0\rangle$ dislocations in Fe–Ni–Cr austenite have their core spread on the $\{1\,1\,1\}$ slip plane with the stacking fault ribbon widths comparable to those predicted by continuum theory. The analysis of dislocation dynamics shows that, at least in the phonon drag regime, the screw dislocations are somewhat less mobile than the edge dislocations.

The addition of nitrogen into Fe–Ni–Cr austenite causes minor changes in the core structure and mobility of the edge dislocation, primarily increasing the frictional stress. In sharp contrast, the interaction of nitrogen atoms with the screw dislocations causes the dislocation core to spread on to two or more planes, and in turn, imparts lower mobility to these dislocations.

Acknowledgements

This work has been supported by the National Science Foundation under Grant DMR-9102973. The author thanks Dr Bruce MacDonald, NSF, for encouragement and continuing interest in the present work, and Drs M. S. Daw and S. M. Foiles for a number of valuable discussions. The encouragement and friendship of Professor W. S. Owen is greatly appreciated.

References

1. M. L. G. BYRNES, M. GRUJICIC and W. S. OWEN, *Acta Metall.* **35** (1987) 1853.
2. J. SASSEN, A. J. GARRATT-REED and W. S. OWEN, in "High Nitrogen Steels, HNS88", edited by J. Foct (The Institute of Metals, London, 1989) p. 1959.
3. M. GRUJICIC, J. C. NILSSON, W. S. OWEN and T. THORVALDSSON, *ibid.* p. 151.
4. M. S. DUESBERY, V. VITEK and D. K. BOWEN, *Proc. Ry. Soc.* **A332** (1973) 85.
5. V. VITEK, R. C. PERRIN and D. K. BOWEN, *Philos. Mag.* **21** (1970) 1049.
6. Z. S. BASINSKI, M. S. DUESBERY and R. TAYLOR, *Can. J. Phys.* **49** (1971) 2160.
7. M. GRUJICIC, *Mater. Sci. Engng* **A183** (1994) 223.
8. R. FLETCHER and C. M. REEVES, *Computer J.* **7** (1964) 149.
9. M. S. DAW and M. I. BASKES, *Phys. Rev. Lett.* **50** (1983) 1285.
10. *Idem*, *Phys. Rev. B* **29** (1984) 6443.
11. M. GRUJICIC and X. W. ZHOU, *Calphad* **17** (1993) 383.
12. E. CLEMENTI and C. ROETTI, "Atomic Data and Nuclear Data Tables", Vol. 14, nos 3 and 4 (Academic Press, New York, 1974).
13. R. W. SMITH and G. S. WAS, *Phys. Rev.* **B40** (1989) 10322.
14. M. GRUJICIC and X. W. ZHOU, *Calphad* **11** (1992) 293.
15. J. P. HIRTH and J. LOTHE, "Theory of Dislocations" (McGraw-Hill, New York, 1968) pp. 315–16.
16. A. SEEGER, *Philos. Mag.* **46** (1955) 1194.
17. M. S. DAW, S. M. FOILES and M. I. BASKES, *Mater. Sci. Rep.* **3** (1993) 253.
18. J. P. HIRTH and J. LOTHE, "Theory of Dislocations" (McGraw-Hill, New York, 1968).
19. P. MUELLNER, C. SOLENTHALER, P. UGGOWITZER and M. O. SPEIDEL, *Mater. Sci. Engng* **A164** (1993) 164.
20. R. SANDSTROM and H. BERGQUIST, *Scan. J. Metal.* **6** (1977) 156.
21. H. M. LEDBETTER, M. W. AUSTIN and S. A. KIM, *Mater. Sci. Engng* **85** (1982) 231.

Received 23 February
and accepted 17 September 1996